

Attractors and chaos of electron dynamics in electromagnetic standing wave

Timur Zh. Esirkepov,¹ Stepan S. Bulanov,² James K. Koga,¹ Masaki Kando,¹
Kiminori Kondo,¹ Nikolay N. Rosanov,^{3,*} Georg Korn,⁴ and Sergei V. Bulanov^{1,†}

¹*QuBS, Japan Atomic Energy Agency, Kizugawa, Kyoto 619-0215, Japan*

²*University of California, Berkeley, CA 94720, USA*

³*Vavilov State Optical Institute, Saint-Petersburg 199034, Russia*

⁴*ELI Beamline Facility, Institute of Physics, Czech Academy of Sciences, Prague 18221, Czech Republic*

The radiation reaction radically influences the electron motion in an electromagnetic standing wave formed by two super-intense counter-propagating laser pulses. Depending on the laser intensity and wavelength, either classical or quantum mode of radiation reaction prevail, or both are strong. When radiation reaction dominates, electron motion evolves to limit cycles and strange attractors. This creates a new framework for high energy physics experiments on an interaction of energetic charged particle beams and colliding super-intense laser pulses.

Keywords: standing wave, radiation reaction, quantum electrodynamics, limit cycle, strange attractor.

PACS numbers: 52.20.Dq, 12.20.-m, 41.60.Ap, 41.75.Ht, 52.27.Ep

arXiv:1412.6028v1 [physics.plasm-ph] 17 Dec 2014

* Also at the ITMO University, Saint-Petersburg 197101, Russia

† Also at A. M. Prokhorov Institute of General Physics of RAS, Moscow, Russia; the ITMO University, Saint-Petersburg 197101, Russia

New regimes of light-matter interaction emerge with the increase of laser power beyond petawatt, leading to radiation pressure dominant acceleration of ions, bright coherent x-ray generation and electron-positron pairs creation [1]. The next generation of high power short-pulse lasers will soon reach the intensity of electromagnetic (EM) radiation of 10^{23} W/cm² for a 1 μ m wavelength [2], 10^5 times greater than the relativistically strong intensity threshold $I_0 = 1.37 \times 10^{18}$ W/cm². Then the EM radiation emission by electrons will be substantial [1, 3, 4], making the electron dynamics strongly dissipative [5, 6] and causing the laser energy fast conversion to hard EM radiation, in the gamma-ray spectral range for typical laser parameters [7, 8].

The laser intensity above 10^{23} W/cm² brings novel physics [9] (see [1, 3, 4, 10–15] for details), where the electron (positron) dynamics is principally determined by the radiation reaction (RR) in its classical form or quantum electrodynamics (QED) effects. The latter weaken the EM emission of relativistic electrons, thus decreasing the classical RR [16, 17].

Even in a simple case of a standing wave (SW), the electron dynamics is surprisingly complicated. At the magnetic field node plane, the electron motion is unstable [11], with the instability growth rate being approximately equal to the EM field frequency. In a linearly polarized SW, the electrons are concentrated in the SW spatial periods [18–20]. The SW configuration is widely used in the QED theory of superstrong EM field interaction with vacuum and charged particles, because the processes description is greatly simplified at the magnetic field node plane: there the electric field vector merely rotates in a circularly polarized (CP) or oscillates in a linearly polarized (LP) SW, with nonzero Poincaré invariants. In addition, the SW formed by two perfectly matched counter-propagating laser pulses has a two times higher electric field than a single laser pulse, which facilitates QED effects as in the multi-beam configuration [21].

In this Letter we show that the SW intensity and wavelength are uncoupled critical parameters determining the electron dynamics in a strong EM SW. The intensity–wavelength plane is divided into four domains where the RR is either negligible, or substantially classical, or mainly manifests itself as a QED effect while the classical RR force is small, or the classical RR force and QED effects are both strong. When the RR is significant, a strongly dissipative motion of electrons results in formation of limit cycles and strange attractors.

The electron dynamics in the EM wave is described by the equation

$$\dot{\mathbf{p}} = e(\mathbf{E} + \boldsymbol{\beta} \times \mathbf{B}) + \mathbf{f}_{\text{rad}}, \quad \mathbf{f}_{\text{rad}} = G_e \mathbf{f}_{\text{LL}}, \quad (1)$$

where $\mathbf{p} = m_e c \gamma_e \boldsymbol{\beta}$, $\boldsymbol{\beta} = \mathbf{v}/c$, $\gamma_e = (1 - \beta^2)^{-1/2}$; \mathbf{E} and \mathbf{B} are the electric and magnetic fields; e , m_e , \mathbf{v} and \mathbf{p} are the electron charge, mass, velocity and momentum; c is the speed of light in vacuum. The RR force in the Landau–Lifshitz form, \mathbf{f}_{LL} [22], is reduced by a factor G_e representing the classical RR weakening due to QED effects, following the approach of Refs. [7, 9, 12].

In the ultrarelativistic limit $\gamma_e \gg 1$, the RR force can be written as

$$\mathbf{f}_{\text{rad}} \approx -\varepsilon_{\text{rad}} G_e m_e c \omega \boldsymbol{\beta} a_S^2 \chi_e^2. \quad (2)$$

Here $\varepsilon_{\text{rad}} = 4\pi r_e/3\lambda \approx 1.18 \times 10^{-8} (1\mu\text{m}/\lambda)$; $r_e = e^2/m_e c^2 \approx 2.82 \times 10^{-13}$ cm is the classical electron radius; $a_S = eE_S/m_e \omega c \approx 4.12 \times 10^5 (\lambda/1\mu\text{m})$ corresponds to the QED critical field $E_S = \alpha e/r_e^2$; $\alpha = e^2/\hbar c$ is the fine-structure constant [23]; ω and λ are the EM wave frequency and wavelength. The relativistic and gauge invariant parameter

$$\chi_e = (\gamma_e/E_S)[(\mathbf{E} + \boldsymbol{\beta} \times \mathbf{B})^2 - (\boldsymbol{\beta} \cdot \mathbf{E})^2]^{1/2} \quad (3)$$

characterizes the probability of a gamma-photon emission by an electron with momentum \mathbf{p} . QED effects are negligible for $\chi_e \ll 1$ and become substantial for $\chi_e \simeq 1$.

The more significant QED effects in the electron motion, the less radiation is emitted. According to [16] the total radiated power is reduced by a factor depending on the parameter χ_e . Introduced in Eq. (2) this factor is written using [23–25] as

$$G_e(\chi_e) = - \int_0^\infty \frac{3 + 1.25\chi_e \xi^{3/2} + 3\chi_e^2 \xi^3}{(1 + \chi_e \xi^{3/2})^4} \text{Ai}'(\xi) \xi d\xi, \quad (4)$$

where $\text{Ai}(x)$ is the Airy function. The photon emission discreet nature is neglected (see [12, 26, 27]). For computations we approximate Eq.(4) by $G_e(\chi_e) \approx (1 + 18\chi_e + 69\chi_e^2 + 73\chi_e^3 + 5.806\chi_e^4)^{-1/3}$, accurate within 10^{-3} for $0 < \chi_e < 10$, with the same asymptotic at 0 and ∞ as Eq. (4).

We consider the electric field of the one-dimensional (1D) CP EM SW near the magnetic field node plane: $\mathbf{a} = -a(\mathbf{i}_2 \cos \tau + \mathbf{i}_3 \sin \tau)$, where \mathbf{i}_2 and \mathbf{i}_3 are orthogonal unit vectors perpendicular to the SW axis; $\tau = \omega t$, $\mathbf{q} = \mathbf{p}/m_e c$, and $a = eE/m_e \omega c = (I/I_0)^{1/2} (\lambda/1\mu\text{m})$. We change to the rotating coordinate system [28],

$$q_{\parallel} = q_2 \cos \tau + q_3 \sin \tau, \quad q_{\perp} = q_2 \sin \tau - q_3 \cos \tau. \quad (5)$$

Eq. (3) yields $\chi_e = (a/a_S)(1 + q_1^2 + q_\perp^2)^{1/2}$.

Substituting Eq. (5) into Eq. (1) and neglecting the electron momentum along the SW axis, $q_1 \ll (q_2^2 + q_3^2)^{1/2}$, we obtain

$$\dot{q}_\parallel + q_\perp = a - \varepsilon_{\text{rad}} G_e(\chi_e) a^2 q_\parallel q_\perp^2 / \gamma_e, \quad (6)$$

$$\dot{q}_\perp - q_\parallel = -\varepsilon_{\text{rad}} G_e(\chi_e) [\gamma_e a + a^2 q_\perp (1 + q_\perp^2) / \gamma_e], \quad (7)$$

where the dot denotes differentiation with respect to τ . Solutions of this system asymptotically tend to steady state (provided $\varepsilon_{\text{rad}} > 0$). Following [6], from Eqs. (6-7) we find the critical EM amplitude determining the RR strength,

$$a_{\text{RQ}} = [\varepsilon_{\text{rad}} G_e(\chi_e)]^{-1/3}. \quad (8)$$

RR is negligible for $a \ll a_{\text{RQ}}$ and becomes substantial for $a \simeq a_{\text{RQ}}$. In this limit, for $q_\perp \propto a_{\text{RQ}}$ with a factor of the order of unity, we estimate the χ_e parameter as $\chi_m \approx a_{\text{RQ}} q_\perp / a_S \approx \eta a_{\text{RQ}}^2 / a_S$ corresponding to $G_m = G_e(\chi_m)$. This gives the critical wavelength at which RR becomes substantially quantum,

$$\lambda_{\text{RQ}} = 9\pi r_e / 2\alpha^3 \chi_m^3 G_m^2. \quad (9)$$

For $\chi_m = 1$ and $G_m \approx 0.18$, we obtain $I_{\text{RQ}} = a_{\text{RQ}}^2 I_0 = 1.75 \times 10^{24}$ W/cm² and $\lambda_{\text{RQ}} = 3.1$ μm .

Taking $d/d\tau = 0$ in Eqs. (6-7), corresponding to the steady state solution [28], we obtain algebraic dependences of q_\parallel, γ_e on q_\perp , and the expression

$$a - q_\perp = [\varepsilon_{\text{rad}} G_e(\chi_e)]^2 a^2 q_\perp^3 (1 + a q_\perp), \quad (10)$$

implicitly defining q_\perp as a function of $a, \varepsilon_{\text{rad}}$, and a_S . Thus all the dependent variables can be represented as functions of the EM SW intensity, $I = E^2 c / 4\pi$, and wavelength, λ . In this way Fig. 1 shows the χ_e parameter, corresponding factor $G_e(\chi_e)$, and the EM SW amplitude normalized to a_{RQ} .

Fig. 1 reveals domains of different role of RR in the model of the electron stationary motion in a rotating electric field. The classical RR effects becomes substantial when $a \gtrsim 0.5 a_{\text{RQ}}$ while QED effects come into play at $\chi_e \gtrsim 0.2$, which corresponds to the classical RR weakening with the factor $G_e \lesssim 0.5$. The intersection of the curves $a/a_{\text{RQ}} = 0.5$ and $\chi_e = 0.2$ gives the characteristic intensity $I_{\text{RQ}}^* \approx 1.5 \times 10^{23}$ W/cm², and wavelength $\lambda_{\text{RQ}}^* \approx 0.76$ μm , within the order of magnitude of the estimate presented above. This is a meeting point of four different domains: RR is negligible in the region I, QED effects dominate while the classical RR force is small in II, RR is mostly classical in III, the classical RR force and QED effects are both strong in IV. Beyond $\chi_e \gtrsim 1$, a discrete nature of electron emission cannot be neglected posing the applicability limit for the model.

In order to generalize the picture given by Eqs. (6-7) and investigate the electron dynamics with RR in classical and QED modes, we numerically simulate the electron motion in a 1D EM SW according to Eqs. (1), (3), (4). In our setting the electric field oscillates at antinodes, $x = \pm n\lambda/2$, and vanishes at nodes, $x = (1/2 \pm n)\lambda/2$, where $n = 0, 1, 2, \dots$. The electron phase space is 6-dimensional, (x, y, z, p_x, p_y, p_z) , however the coordinates y and z are *ignorable* (do not influence the dynamics), because the EM field depends only on (t, x) . In a LP SW where the electric field is polarized along z -axis, the equation for the y -component of the electron momentum contains only dissipative terms, thus p_y is exponentially dumped, in general. This allows us to restrict the presentation of the electron trajectories to the phase subspace (x, p_x, p_z) for LP SW, and to (x, p_y, p_z) for CP SW.

Fig. 2 shows data for electrons moving in a LP or CP EM SW at different intensity, I , and wavelength, λ , varying as follows: I from $10^3 I_0 = 1.37 \times 10^{21}$ to $10^7 I_0 = 1.37 \times 10^{25}$ W/cm² and λ from 0.1 to 10 μm . Electrons with zero momentum are initially located within the SW spatial period, $0 < x_0/\lambda < 1/2$. They remain confined in this interval or escape, depending on the EM SW intensity and wavelength. Hatched regions in Fig. 2(a,b) indicate I and λ , at which escaping electrons appear. Such electrons perform a “random walk” motion: they travel over large distances migrating between SW spatial periods sometimes oscillating near the electric field node planes [19, 29]. The boundary between the regions of escaping and confined trajectories roughly corresponds to the curve $a = 0.5 a_{\text{RQ}}$ in Fig. 1.

When the RR becomes significant, the dissipation contracts the possible volume occupied by trajectories, resulting in trapping of electrons within the SW spatial period. Fig. 2(a,b) presents the maximum Lorentz factor, γ_e , and the maximum χ_e parameter reached by electrons on their trajectories.

Fig. 2(c-f) shows the characteristics of confined trajectories (white regions indicate escaping trajectories). The maximum χ_e parameter obtained on the trajectories originated at x_0 is shown in Fig. 2(c,d) for the SW wavelength of $\lambda = 1$ μm . Trajectories starting near the electric field node exhibit lower χ_e values. Frame (e) shows the time-averaged longitudinal coordinate, \bar{x} , of the trajectories originated at x_0 in the LP SW. Electrons fall into few attractors near the electric field nodes and antinodes, where they perform quasi-periodic oscillations. The same style frame for the CP SW would be homogeneous in color since all the trajectories in the CP SW, if they are confined in the SW spatial

period, reduce to low-magnitude oscillations near the electric field node (see Fig. 3). Therefore in (f) we present the duration of a circular motion, t_{circ} , for trajectories originated very close to the electric field antinode. The maximum γ_e and χ_e distribution on the (I, λ) plane for an asymptotic motion of confined electrons is almost the same as (a) for LP SW and very much different form (b) for CP SW, where the asymptotic motion is weakly relativistic. The time-average power of EM radiation emitted by an electron on its trajectory is shown in (e,f) by black curves. For LP SW (e) it is for an asymptotic motion while for CP SW (f) it is for the initial circular motion near the electric field antinode. The higher the CP SW amplitude, the longer the circular motion.

Typical electron trajectories in the phase space for the LP and CP SW are exemplified in Fig. 3, for $I = 1.37 \times 10^{24}$ W/cm², $\lambda = 1 \mu\text{m}$. Due to a strong dissipation, electrons started with different momenta, Fig. 3(a,f), quickly fall to an asymptotic motion near attractors. In the LP SW, Fig. 3(a), electrons fall into different attractors depending on their initial coordinate and momentum (as was seen in Fig. 2(e)). In the CP SW, Fig. 3(f), electrons fall into a single attractor at the electric field node irrespective of the initial coordinate and momentum. However, if electrons were initially sufficiently close to the electric field antinode, then before falling into the attractor they perform few rotations emitting all the power received from the CP SW, as seen in Fig. 2(f).

In the LP SW, near the electric field antinode there are limit cycles Fig. 3(b,c), characterized by a large values of γ_e , χ_e and time-averaged emitted power, Fig. 2(a,c,e). Near the electric field node we see a bow-like limit cycle Fig. 3(d) with relatively high $\chi_{e \text{ max}} \sim 3$, and a knot-like attractor Fig. 3(e), much weaker in terms of p_x, p_z . Due to the symmetry of motion equations, a confined trajectory has a twin which is antisymmetric in the phase space with respect to the electric field node. The oscillations near the electric field node exhibit substantial frequency upshift, so that electron trajectory makes many cycles around the fixed point $x/\lambda = 1/4$ during one time cycle of the LP SW. The analysis of linearized motion equations shows that in this case the electron dynamics is characterized by two timescales, one corresponding to the SW frequency and another being determined by the SW amplitude and the electron Lorentz factor.

In the CP SW, Fig. 3(f), all the trajectories fall into one of an infinite system of limit cycles near the electric field node, which forms a pompom-like structure Fig. 3(g). Here $\chi_e \ll 1$.

The kind and localization of attractors strongly depend on the SW intensity and wavelength. For the same intensity of $I = 1.37 \times 10^{24}$ W/cm², the case of $\lambda = 3 \mu\text{m}$ shows different limit cycles near the electric field antinodes but the same type attractors near nodes. When $\lambda = 0.3 \mu\text{m}$, the classical RR force is strongly weakened by the QED effects, so the confined trajectories chaotically jump between different types of oscillations resembling motion near attractors seen at higher λ .

The attractors near the electric field node in LP and CP SW exhibit properties of strange attractors, playing a fundamental role in the theory of dynamic systems [30]. As numerical analysis shows, the trajectories near the electric field node behave as dense periodic orbits. The trajectories in the LP SW starting with a zero momentum from x_0 corresponding to the time-average $\bar{x} \approx 1/4$, yellow region in Fig. 2(e), and trajectories in the CP SW starting near $x_0 = 1/4$ are highly sensitive to the initial coordinate. More precisely, the indication of the presence of strange attractors is given by the maximal Lyapunov exponent [30],

$$\Lambda = \lim_{t \rightarrow \infty} t^{-1} \lim_{\delta_0 \rightarrow 0} \ln[\delta(t)/\delta_0], \quad (11)$$

where $\delta(t)$ is the distance in the phase space between the ends of two trajectories, initially separated by $\delta_0 = \delta(0)$. For the attractor in the LP SW, shown in Fig. 3(e), the maximum Lyapunov exponent numerically estimated as $\Lambda \gtrsim 5$, and for the CP SW case, shown in Fig. 3(g), as $\Lambda \gtrsim 1$. Since they are both positive, the trajectories confined near the electric field node are chaotic, revealing strange attractors.

According to our numerical analysis, confined motion of electrons near the electric field nodes and antinodes is robust with respect to small imbalances of the intensity and wavelength of EM waves forming the SW. Even though the nodes and antinodes are no longer stationary in this case, the asymptotic motion resembles oscillations near attractors, slowly drifting along the x -axis during an oscillation cycle.

This robustness also manifests itself when a transient standing wave is formed by two counter-propagating paraxial gaussian laser beams with the intensity $I = (1.37/4) \times 10^{24}$ W/cm², wavelength $\lambda = 1 \mu\text{m}$, duration $10\lambda/c = 33$ fs and focal spot $3 \mu\text{m}$, Fig. 4. The constructive interference of these two paraxial pulses gives the SW peak intensity of $I = 1.37 \times 10^{24}$ W/cm².

Initially (at $t = -20\lambda/c$) randomly distributed in the box $[-1.5, 1.5]^3 \lambda^3$, 10^3 electrons move in the transient SW, which is formed around $t = 0$ for approximately $3\lambda/c$. About 10% and 15% electrons remain in the box for more than 25 laser cycles in the LP and CP SW, respectively. Their trajectories are exemplified in Fig. 4(a,d). These trajectories fall into attractors typical for a 1D SW, although somewhat displaced due to non-stationary location of peripheral nodes and antinodes. In the LP case, we see limit cycles near the electric field nodes and a knot-like attractors at antinodes, Fig. 4(b,c). In the CP case, we see pompom-like attractors at antinodes, Fig. 4(e,f).

In conclusion, in the electron dynamics in a strong electromagnetic standing wave, the electromagnetic wave intensity $I_{\text{RQ}} \sim 10^{24}$ W/cm² and wavelength $\lambda_{\text{RQ}} \sim 1 \mu\text{m}$, reachable in near future by high-power lasers [2], separate different

regimes of radiation reaction. For $I < I_{\text{RQ}}$ and $\lambda > \lambda_{\text{RQ}}$, it is possible to achieve strong classical RR force without significant QED effects, whereas for $I > I_{\text{RQ}}$ and $\lambda < \lambda_{\text{RQ}}$, strong QED effects can be seen with a relatively small classical RR force.

When radiation reaction is significant, a strong dissipation results in formation of limit cycles and strange attractors, depending on the standing wave polarization. A high energy and χ_e parameter are achieved on limit cycles near the electric field antinode in the linearly polarized standing wave.

When a transient standing wave is formed by two intense counter-propagating laser pulses, a substantial number of electrons is confined for the standing wave lifetime ($\approx 1/3$ of a Gaussian laser pulse duration), tracing limit cycles and strange attractors peculiar to ideal planar standing wave. Since electrons forget their initial momenta due to dissipation, the interaction of a GeV electron beam transversely propagating through a collision point of two multi-petawatt counter-propagating laser pulses can create a *transient microscopic storage ring* similar to a synchrotron, which reveals itself by a characteristic transverse high-power high-frequency electromagnetic radiation and the resulting spatial and spectral electron distribution. This creates a new framework for high energy physics experiments, in particular, solving a well-known problem of charged particles delivery to the highest intensity region of the electromagnetic field.

ACKNOWLEDGMENTS

We thank M. Jirka, O. Klimo, S. Weber, and A. G. Zhidkov for discussions. S.V.B. and T.Z.E. acknowledge support from ELI-Beamlines.

-
- [1] G. A. Mourou, T. Tajima, S. V. Bulanov, *Rev. Mod. Phys.* **78**, 309 (2006).
 - [2] G. A. Mourou, et al. (Eds) ELI - Extreme Light Infrastructure Science and Technology with Ultra-Intense Lasers WHITE-BOOK (Berlin: THOSS Media GmbH, 2011).
 - [3] M. Marklund, P. Shukla, *Rev. Mod. Phys.* **78**, 591 (2006).
 - [4] A. Di Piazza, et al., *Rev. Mod. Phys.* **84**, 1177 (2012).
 - [5] A. Zhidkov, et al., *Phys. Rev. Lett.* **88**, 185002 (2002).
 - [6] S. V. Bulanov, et al., *Plasma Phys. Rep.* **30**, 196 (2004).
 - [7] C. P. Ridgers, et al., *Phys. Rev. Lett.* **108**, 165006 (2012).
 - [8] T. Nakamura, et al., *Phys. Rev. Lett.* **108**, 195001 (2012).
 - [9] A. R. Bell, J. G. Kirk, *Phys. Rev. Lett.* **101**, 200403 (2008).
 - [10] A. M. Fedotov, et al., *Phys. Rev. Lett.* **105**, 080402 (2010).
 - [11] S. S. Bulanov, et al., *Phys. Rev. Lett.* **105**, 220407 (2010).
 - [12] S. S. Bulanov, et al., *Phys. Rev. A* **87**, 062110 (2013).
 - [13] A. Zhidkov, et al., *Phys. Rev. STAB* **17**, 054001 (2014).
 - [14] N. V. Elkina, et al., *Phys. Rev. E* **89**, 053315 (2014).
 - [15] M. Vranic, et al., *Phys. Rev. Lett.* **113**, 134801 (2014).
 - [16] J. Schwinger, *Proc. Natl. Acad. Sci. U.S.A.* **40**, 132 (1954).
 - [17] A. A. Sokolov, N. P. Klepikov, I. M. Ternov, *Sov. Phys. JETP* **24**, 249 (1954).
 - [18] L. L. Ji, et al., *Phys. Rev. Lett.* **112**, 145003 (2014).
 - [19] A. Gonoskov, et al., *Phys. Rev. Lett.* **113**, 014801 (2014).
 - [20] N. Neitz, A. Di Piazza, *Phys. Rev. Lett.* **111**, 054802 (2014).
 - [21] S. S. Bulanov, et al., *Phys. Rev. Lett.* **104**, 220404 (2010).
 - [22] L. D. Landau, E. M. Lifshitz, *The Classical Theory of Fields* (Pergamon, Oxford, 1975), §76.
 - [23] V. B. Berestetskii, E. M. Lifshitz, L. P. Pitaevskii, *Quantum Electrodynamics* (Pergamon, Oxford, 1982).
 - [24] V. I. Ritus, in *Issues in Intense-Field Quantum Electrodynamics* (Nova Science, Commack, 1987).
 - [25] I. V. Sokolov, et al., *Phys. Rev. E* **81**, 036412 (2010).
 - [26] R. Duclous, J. G. Kirk, A. R. Bell, *Plasma Phys. Contr. Fusion* **53**, 015009 (2011).
 - [27] C. S. Brady, et al., *Phys. Rev. Lett.* **109**, 245006 (2012).
 - [28] S. V. Bulanov, et al., *Phys. Rev. E* **84**, 056605 (2011).
 - [29] S. V. Bulanov, et al., *Plasma Phys. Rep.* **41**, 1 (2015).
 - [30] J. R. Eckmann, D. Ruelle, *Rev. Mod. Phys.* **57**, 617 (1985).

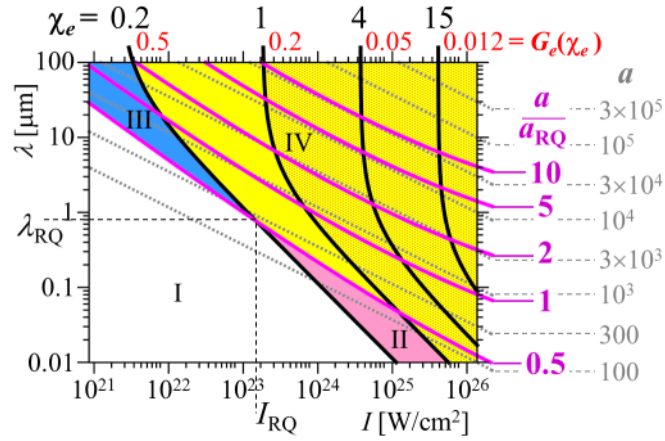


FIG. 1. (color). Stationary motion of electron in a rotating electric field with the dimensionless amplitude a (gray dashed curves): χ_e parameter (black curves) and corresponding factor $G_e(\chi_e)$ (red), and the amplitude normalized to $a_{\text{RQ}} = [\varepsilon_{\text{rad}} G_e(\chi_e)]^{-1/3}$ (magenta curves), versus the electric field intensity, I , and wavelength, λ . Radiation reaction (RR) is negligible in the region I, QED effects dominate while the classical RR force is small in II, RR is mostly classical in III, the classical RR force and QED effects are both strong in IV. Hatched region where discrete nature of electron emission cannot be neglected.

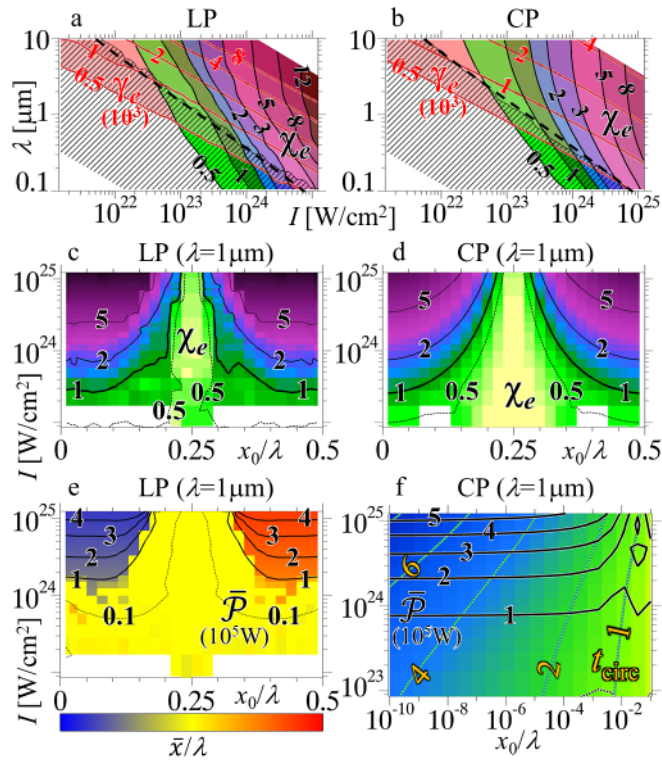


FIG. 2. (color). The maximum Lorentz factor, γ_e (red curves) and the maximum χ_e parameter (black curves) and escaping trajectories (hatched region) in the linearly (a, LP) and circularly (b, CP) polarized standing waves (SW) versus the wave intensity, I , and wavelength, λ . Dashed lines for $I \times (\lambda/1\mu\text{m})^{1.6} = 2 \times 10^{23} \text{ W/cm}^2$. The maximum χ_e parameter (curves and colorscale) on the trajectories originated at x_0 in the LP (c) and CP (d) SW for $\lambda = 1\mu\text{m}$. The time-averaged longitudinal coordinate (\bar{x} , colorscale) of the trajectories originated at x_0 in the LP SW (e) and the duration of a circular motion (t_{circ} , in wave periods, dashed curves and colorscale) for CP SW (f), for $\lambda = 1\mu\text{m}$. Black curves in (e), (f) for the time-average emitted power in 10^5 W .

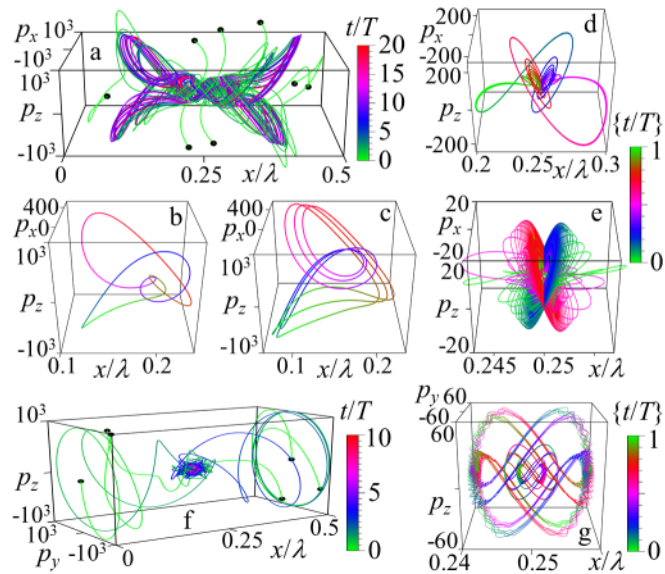


FIG. 3. (color). Typical electron trajectories and attractors in linear (a-e) and circular (f,g) polarized standing wave for $I = 1.37 \times 10^{24}$ W/cm², $\lambda = 1\mu\text{m}$. Black dots (a,f) for initial locations. Color for time in wave periods; in (b-e,g) denote the fractional part.

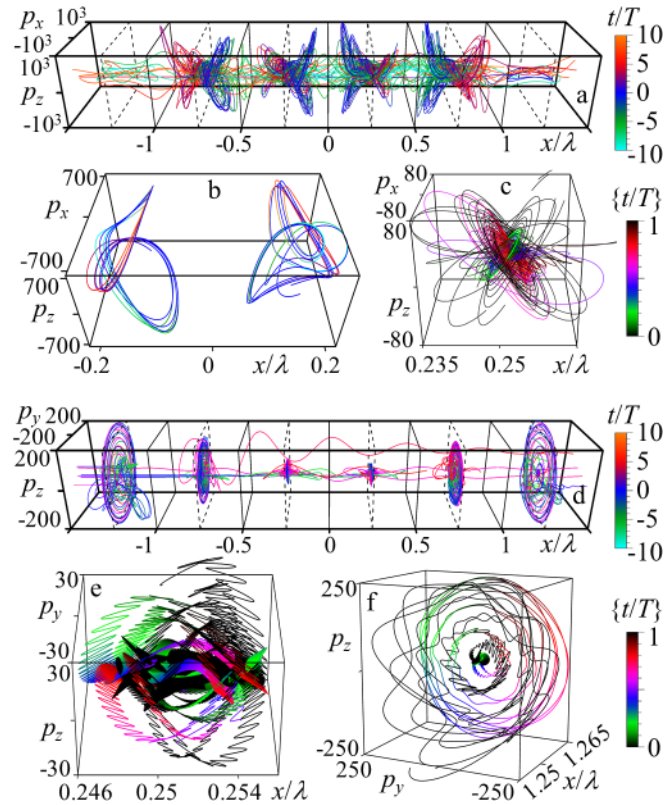


FIG. 4. (color). The electron trajectories in the standing wave formed by two colliding linearly (a,b,c, LP) and circularly (d,e,f, CP) polarized laser pulses propagating along x -axis and having $I = 1.37 \times 10^{24}$ W/cm², $\lambda = 1\mu\text{m}$, duration 33 fs and focal spot $3\mu\text{m}$.